Electronic Supplementary Information (ESI)

In situ synthesis of Co-B-doped porous carbon through laser thermal reduction for the efficient oxygen reduction reaction

Junbo Liu[a], Wenzhuo Zhang[b], Guangyi Chen[c] and Shengyang Tao*[a]

[a] Department of Chemistry, School of Chemical Engineering, Dalian University of Technology, Dalian, Liaoning, P. R. China.

*Corresponding author. E-mail: taosy@dlut.edu.cn

1. Finite-element Simulation Analysis

A laser beam moved on the BPR substrate doped with Co_3O_4 nanoparticles to synthesize a Co/B-C catalyst. P was the laser power. The surface absorptivity of the BPR substrate was recorded as ε. We assumued that the absorptivity was equal to the emissivity. The transient temperature of the laser spot could be analyzed by finite-element simulation.

The temperature of the surface of the BPR substrate was determined by the incident heat flux of the laser. We assumed that the BPR substrate was opaque in the operating wavelength range of the laser, indicating that no light penetrated the BPR substrate. All the heat generated by the laser was absorbed by the BPR film.

The energy conservation law as follows:

$$\rho C_{\mathrm{p}} \frac{\partial T}{\partial t} + \rho C_{\mathrm{p}} u \cdot \nabla T + \nabla \cdot q = Q + Q_{\mathrm{ted}} \tag{1}$$

Where ρ is the density of BPR, C_{p} is the constant pressure heat capacity, T is temperature, t is time. Heat flux q ($\mathrm{W \cdot m^{-2}}$) is defined as $q = -\kappa \nabla T$, here κ ($\mathrm{W \cdot m^{-1} k^{-1}}$) is heat conductivity.

The laser thermal load should be multiplied by ε. Heat flux of the surface of the BPR substrate is defined as $q_0 = \varepsilon \times q$.

2. Electrochemical characterization

The oxygen reduction reaction (ORR) was evaluated with a rotating disk electrode (RDE, with a diameter of 5.0 mm) and a rotating ring-disk electrode (RRDE, Pt ring, with a disc diameter of 5.61 mm, a ring inner diameter of 6.25 mm, and a ring outer diameter of 7.92 mm) setup from Pine Instrument Company connected to the CHI 760E electrochemical workstation (Shanghai Chenhua Instrument Co., Ltd).

The electrochemical test was carried out at room temperature with a conventional three-electrode system, a saturated Ag/AgCl as the reference electrode, platinum as the counter electrode, and a glass carbon (GC) substrate with different catalysts as the working electrode.

The catalyst (5mg) and Nafion (10 μL, 5 wt%) were dispersed in 1 mL ethanol/deionized water (volume ratio, 3:1) solution, followed by ultrasonication for 20 min to get a uniform suspension. Then, catalyst inks (5 μL) were dropped onto the GC electrode and further dried for 12 h at room temperature as the working electrode.

All potentials in this study were measured against the Ag/AgCl reference electrode and converted to the reversible hydrogen electrode (RHE) according to the Nernst equation: $E\ (RHE) = E\ (Ag/AgCl) + 0.059 \times pH + 0.199$ V.

Linear sweep voltammetry (LSV) was measured in O_2-saturated 0.1 mol L^{-1} KOH solution at a sweep rate of 5 mV s^{-1} with different rotating speed (400, 800, 1200, 1600, and 2000 rpm). The scanning potential was from -1.0 to 0 V (vs. Ag/AgCl) and the ring potential was constant at 0.3 V (vs. Ag/AgCl).

The transferred electron numbers (n) were first determined by the Koutecky-Levich (K-L) equation:

$$\frac{1}{J}=\frac{1}{J_K}+\frac{1}{J_L}=\frac{1}{J_K}+\frac{1}{B\omega^{1/2}}$$

$$B = 0.62nFC_0D_0^{2/3}v^{-1/6}$$

$$J_K=\frac{J\times J_L}{J_L-J}$$

Where J is the measured current density (mA cm^{-2}), J_K and J_L are the kinetic and diffusion-limiting current densities, ω is the angular velocity of the disk (rad s^{-1}), n is the electron transfer number, F is the Faraday constant (96485 C mol^{-1}), C_0 (1.2×10^{-6} mol cm^{-3}) is the bulk concentration of O_2, D_0 (1.9×10^{-5} cm^2 s^{-1}) is the diffusion coefficient of O_2 in 0.1 M KOH, and v (0.01 cm^2 s^{-1}) is the kinetic viscosity of the electrolyte.

The hydrogen peroxide yield (H_2O_2%) and the electron transfer number (n) were determined by the following equations:

$$H_2O_2\% = 200\times\frac{I_r/N}{I_d+I_r/N}$$

$$n = 4\times\frac{I_d}{I_d+I_r/N}$$

where I_d is the disk current, I_r is the ring current, and N (0.37) is the current collection efficiency of the Pt ring. LSV measurement for the current collection efficiency was conducted in $K_3Fe[CN]_6$ solution.

Cyclic voltammograms (CVs) were recorded from -1.0 to 0 V (vs. Ag/AgCl) in N_2 and O_2-saturated 0.1 mol L^{-1} KOH solution at a sweep rate of 50 mV s^{-1}. Chronoamperometry curves were recorded at a constant working potential of -0.3 V (vs. Ag/AgCl) for 10000 s to evaluate the durability of catalysts. Electrochemical impedance spectra (EIS) were measured at open potential under the frequency from 0.1 Hz to 100 kHz.

3. Supplementary Figures

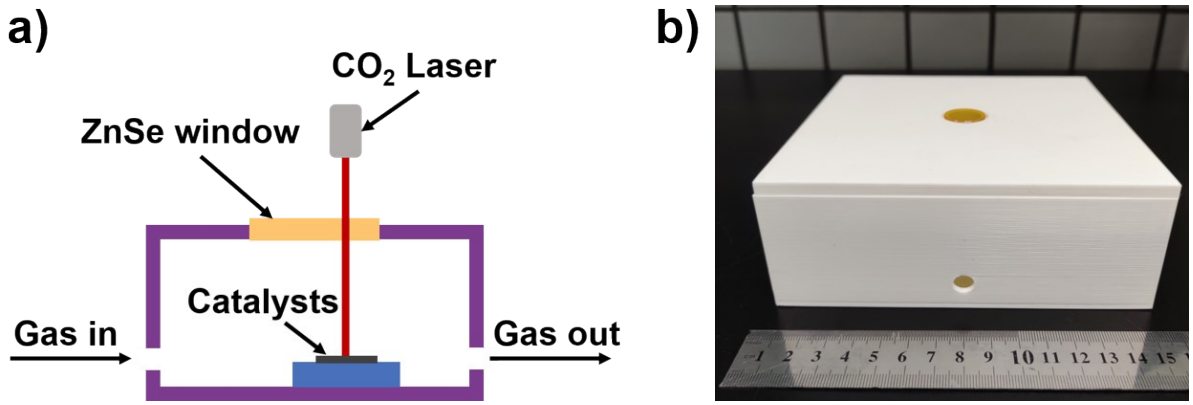

Fig. S1. (a) Schematic illustration of N-doped catalysts by the LTR process in N_2 atmosphere. (b) Photograph of gas atmosphere box produced by a 3D printer.

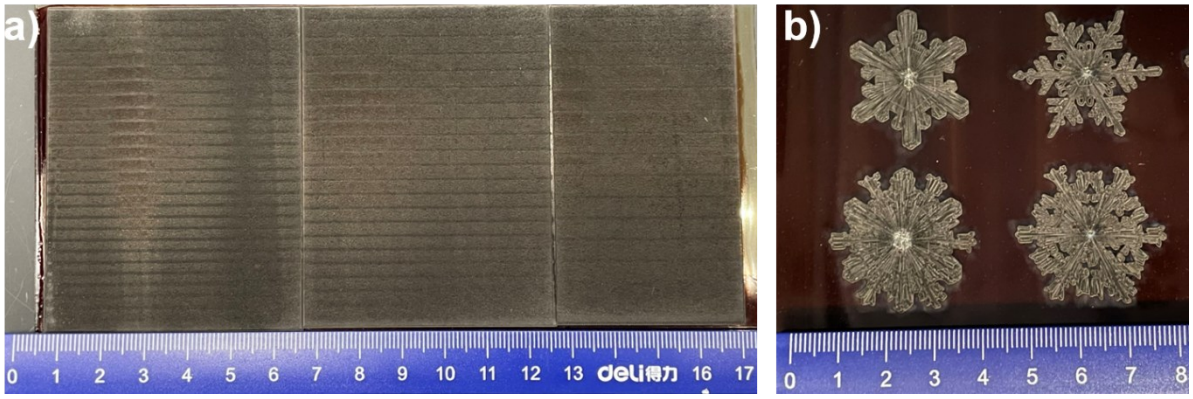

Fig. S2. (a)The surface of catalyst with an area of about 130 cm^2. (b) Various Snowflake patterns on BPR film.

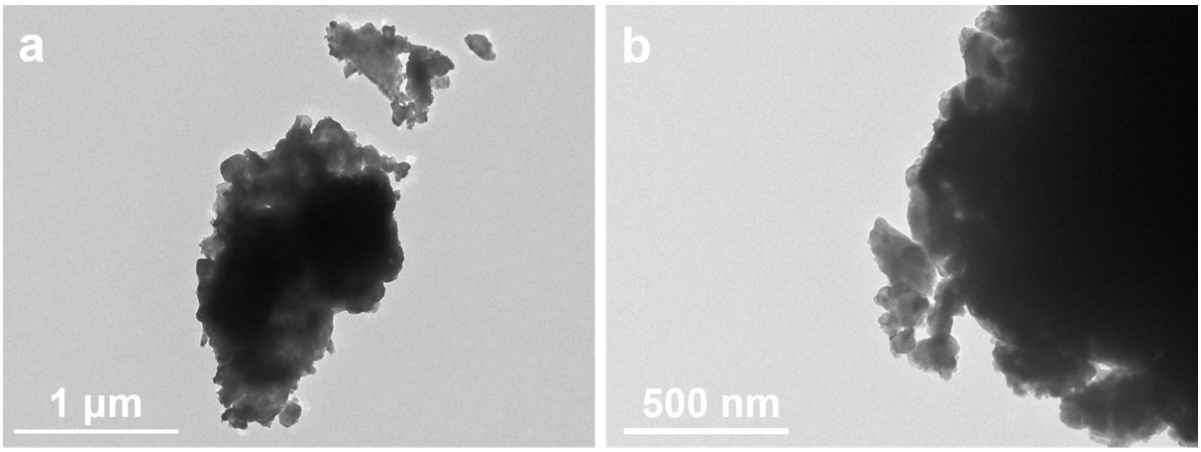

Fig. S3. (a,b)The TEM images of the carbon synthesized by muffle furnace.

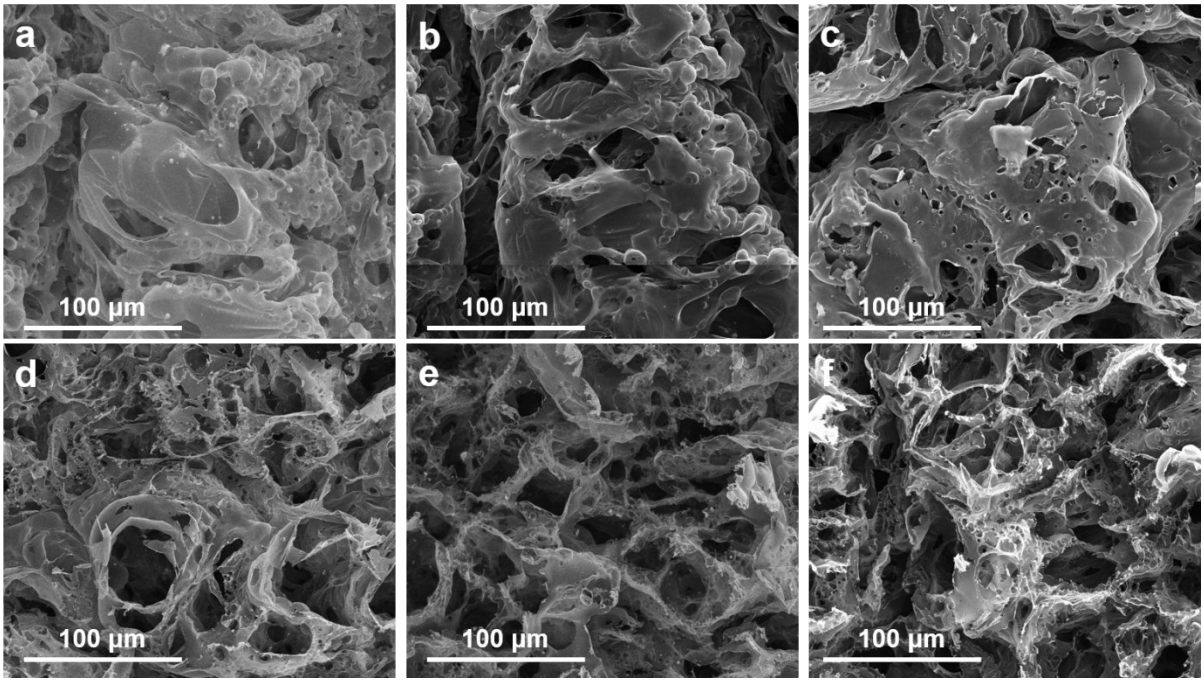

Fig. S4. SEM images of the hybrid Co/B-C catalysts formed at different laser powers: (a) 4.5 W, (b) 6 W, (c) 9 W, (d) 12 W, (e) 15 W, and (f) 18 W.

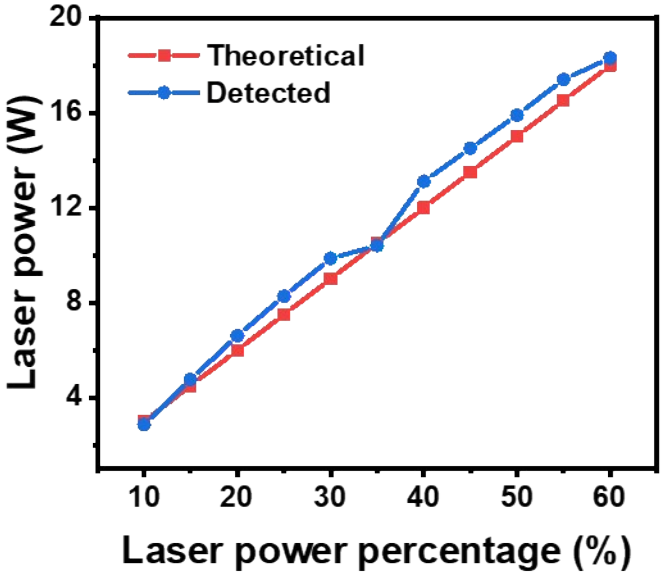

Fig. S5. The laser power of theoretically calculated and experimentally measured under incandescent lamps at night.

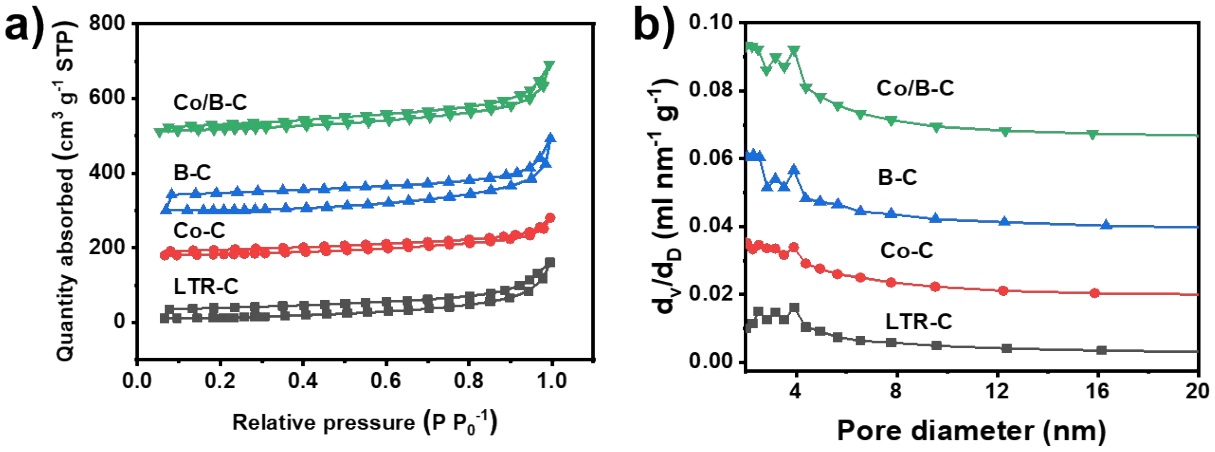

Fig. S6. (a) N_2 adsorption-desorption isotherms of various catalysts (red line, blue line, and green line are shifted by 130, 295, and 475 cm^3 g^{-1} STP for clarity, respectively). (b) BJH pore size distributions.

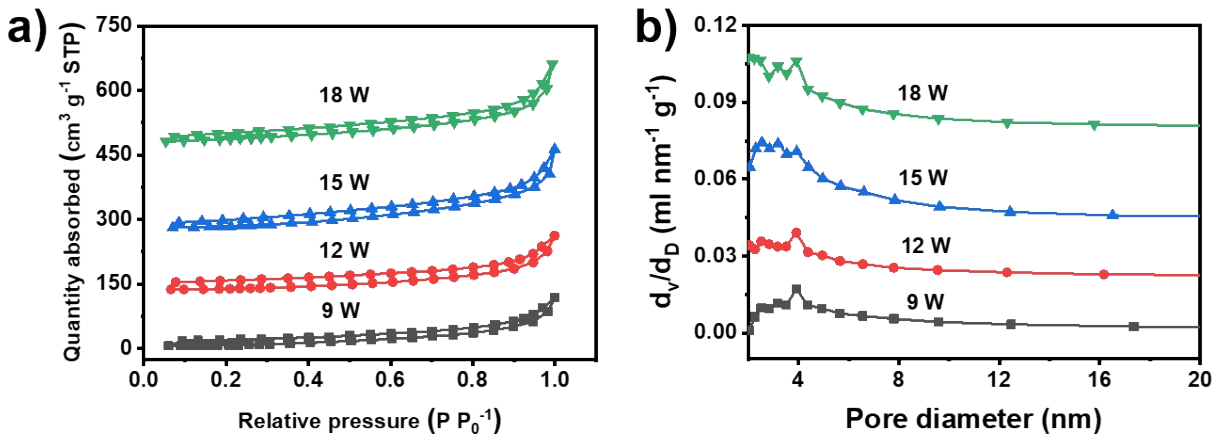

Fig. S7. (a) N_2 adsorption-desorption isotherms of the hybrid Co/B-C catalysts prepared with different laser power (red line, blue line, and green line are shifted by 130, 275, and 445 cm^3 g^{-1} STP for clarity, respectively). (b) BJH pore size distributions.

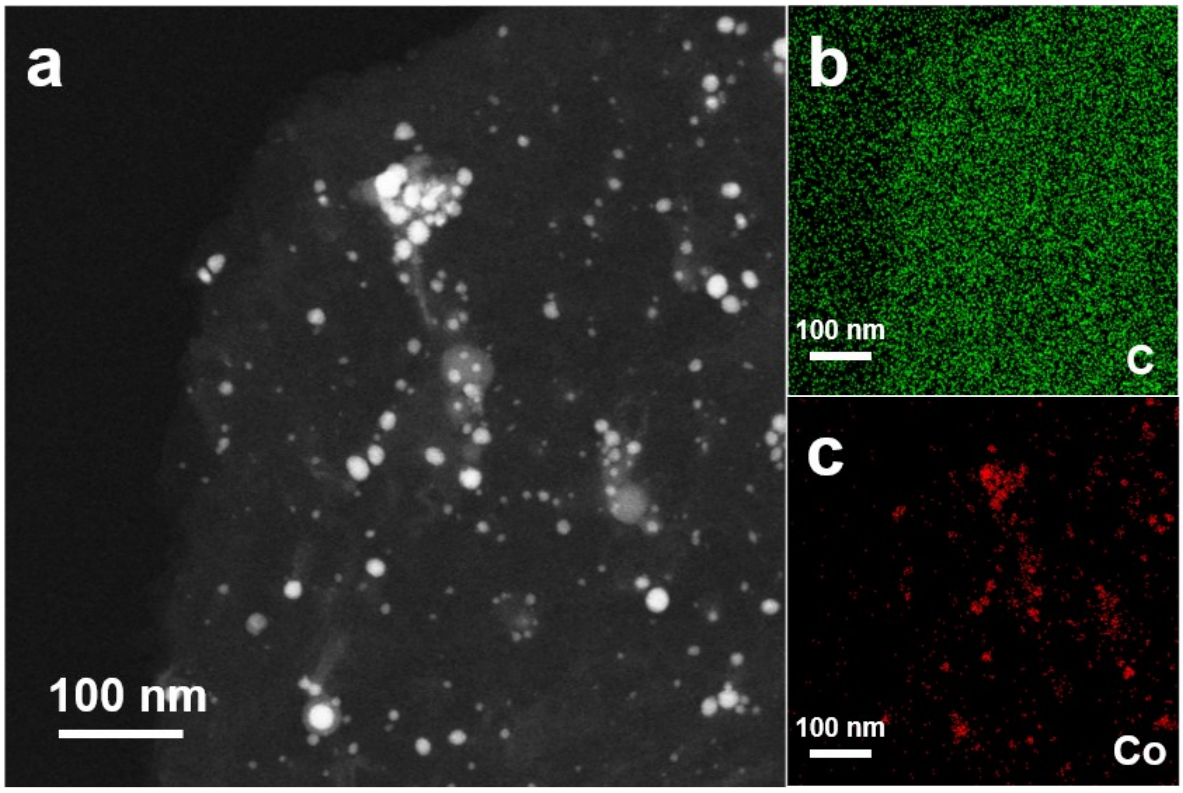

Fig. S8. (a) HRTEM image of the hybrid Co/B-C catalyst. Elemental mapping of (b) C and (c) Co of the hybrid Co/B-C catalyst.

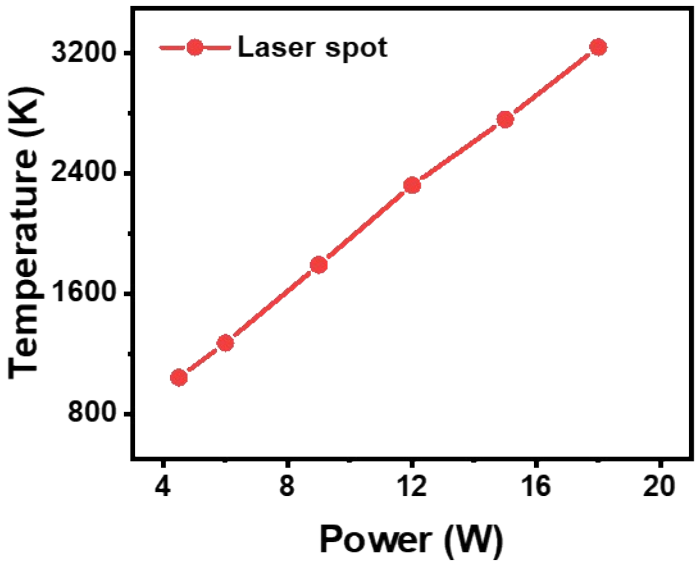

Fig. S9. The temperature of a laser spot on the surface of the BPR at different laser power based on finite element simulation.

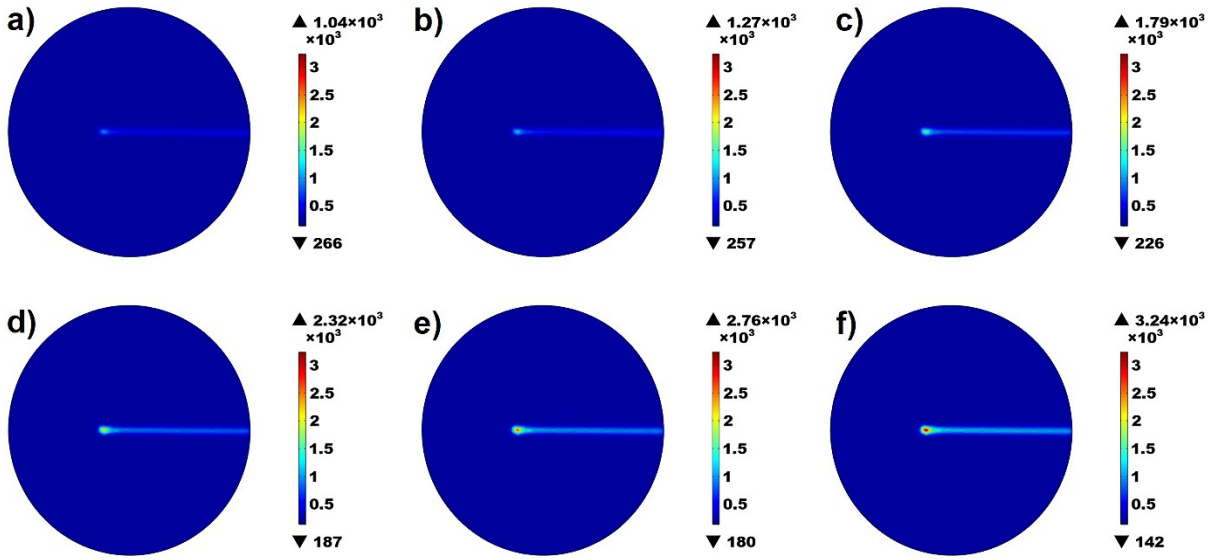

Fig. S10. The temperature mapping of laser path: (a) 4.5 W, (b) 6 W, (c) 9 W, (d) 12 W, (e) 15 W, and (f) 18 W.

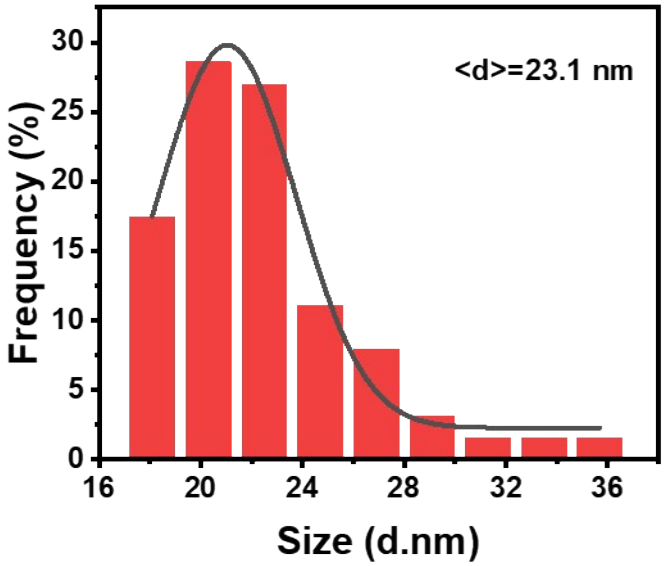

Fig. S11. The particle size distribution of the Co NPs measured on HRTEM image of Co/B-C prepared by 18 W.

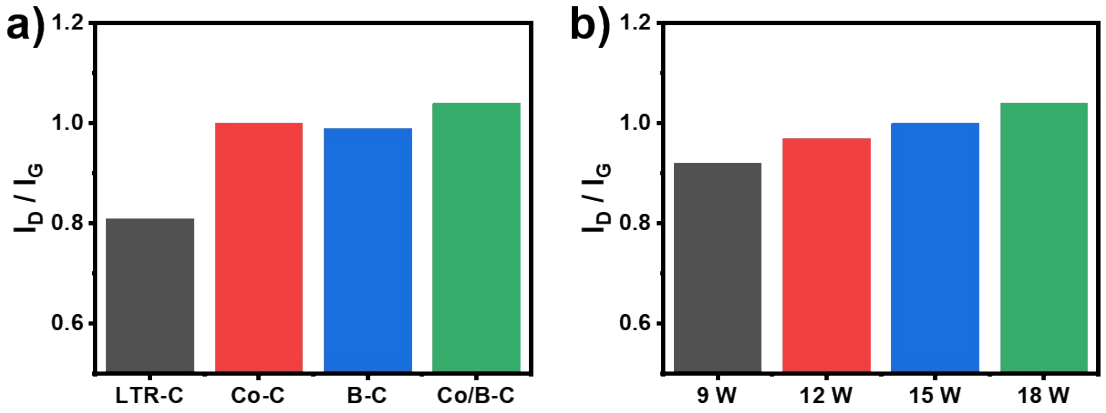

Fig. S12. (a) The intensity ratio of I_D/I_G peak according to Fig. 4c. (b) The intensity ratio of I_D/I_G peak according to Fig. 4d.

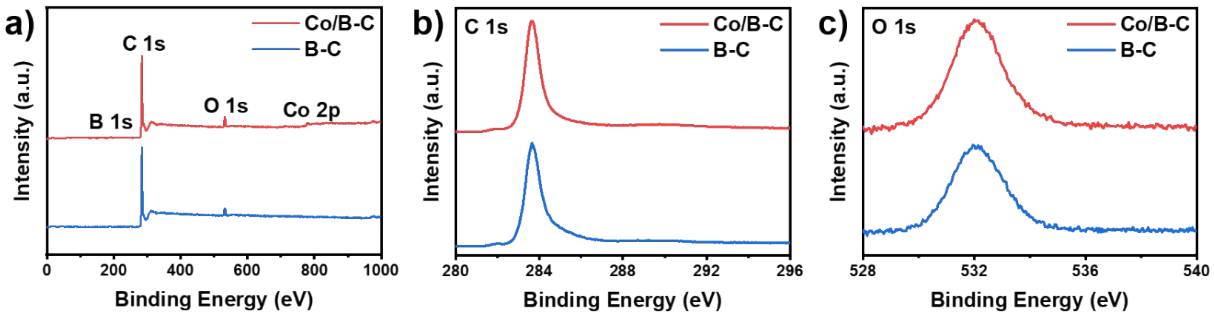

Fig. S13. (a) XPS survey spectra of Co/B-C and B-C catalysts. High-resolution XPS spectra of (b) C 1s, (c) O 1s.

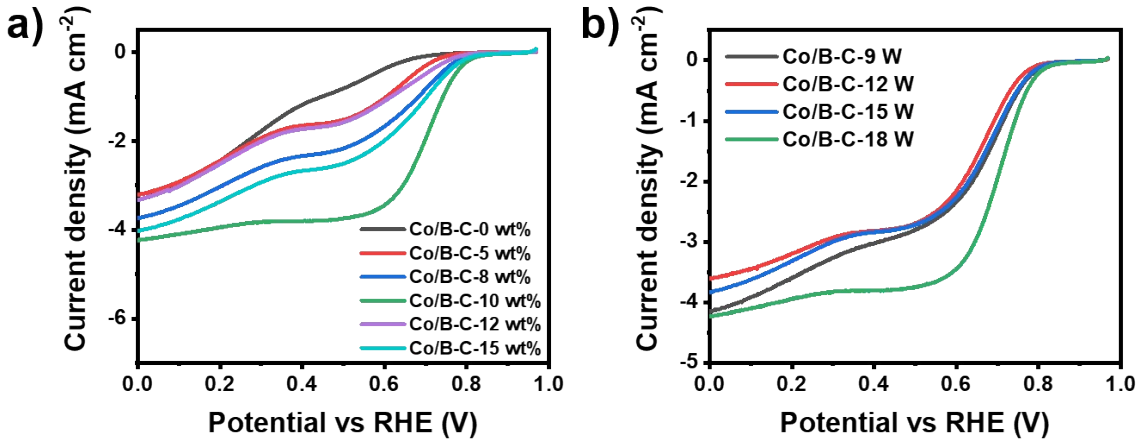

Fig. S14. (a) The LSV curves of the hybrid Co/B-C catalysts synthesized by different doping amounts of Co_3O_4 NPs. (b) The LSV curves of the hybrid Co/B-C catalysts synthesized by different laser power.

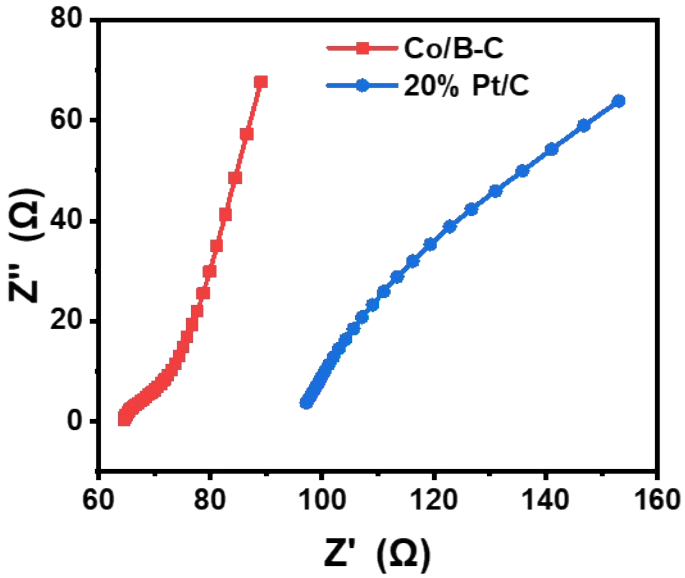

Fig. S15. Nyquist curves of the hybrid Co/B-C and commercial 20% Pt/C catalysts in the range of 0.1 Hz to 10^5 Hz.

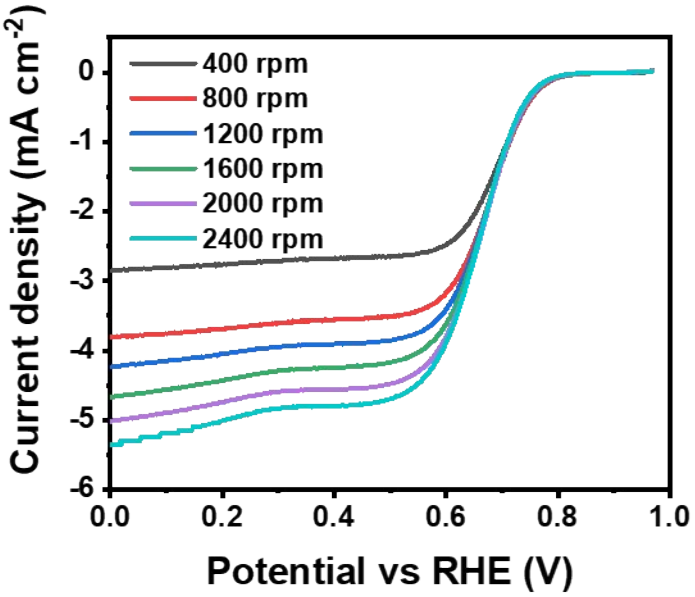

Fig. S16. LSV curves of the hybrid Co/B-C catalyst at various rotating speeds in O_2-saturated 0.1 M KOH.

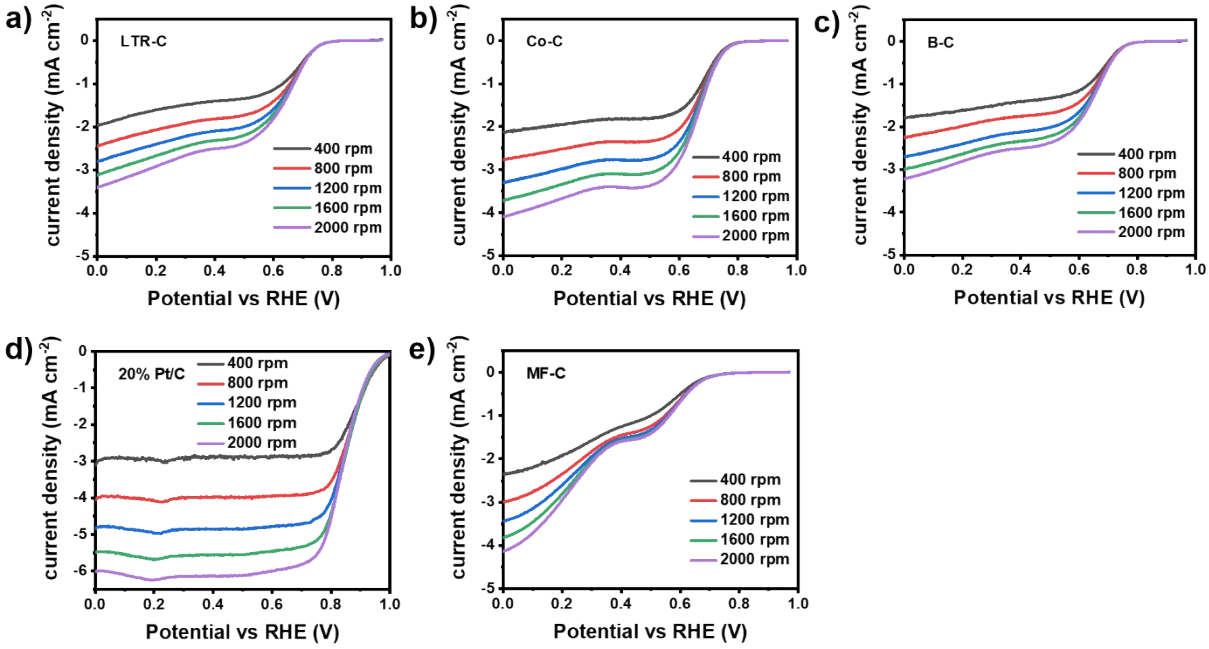

Fig. S17. LSV curves of the as-synthesized catalysts at various rotating speeds in O_2-saturated 0.1 M KOH. (a) Carbon obtained from PR using a CO_2 laser. (b) Co-C catalyst. (c)B-C catalyst. (d) Commercial 20% Pt/C catalyst. (e) Carbon synthesized by muffle furnace.

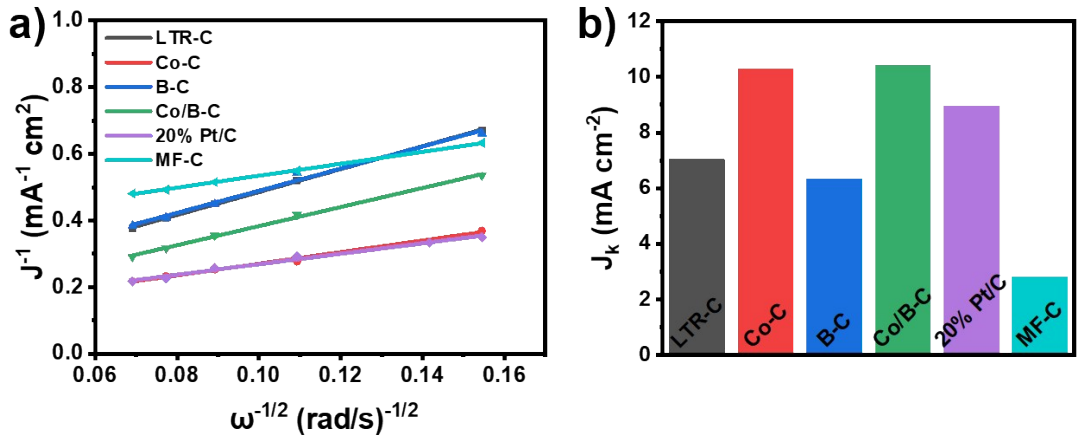

Fig. S18. (a) K-L plots of various catalysts at 0.3 V. (b) Summarized kinetic current of various catalysts at 0.3 V.

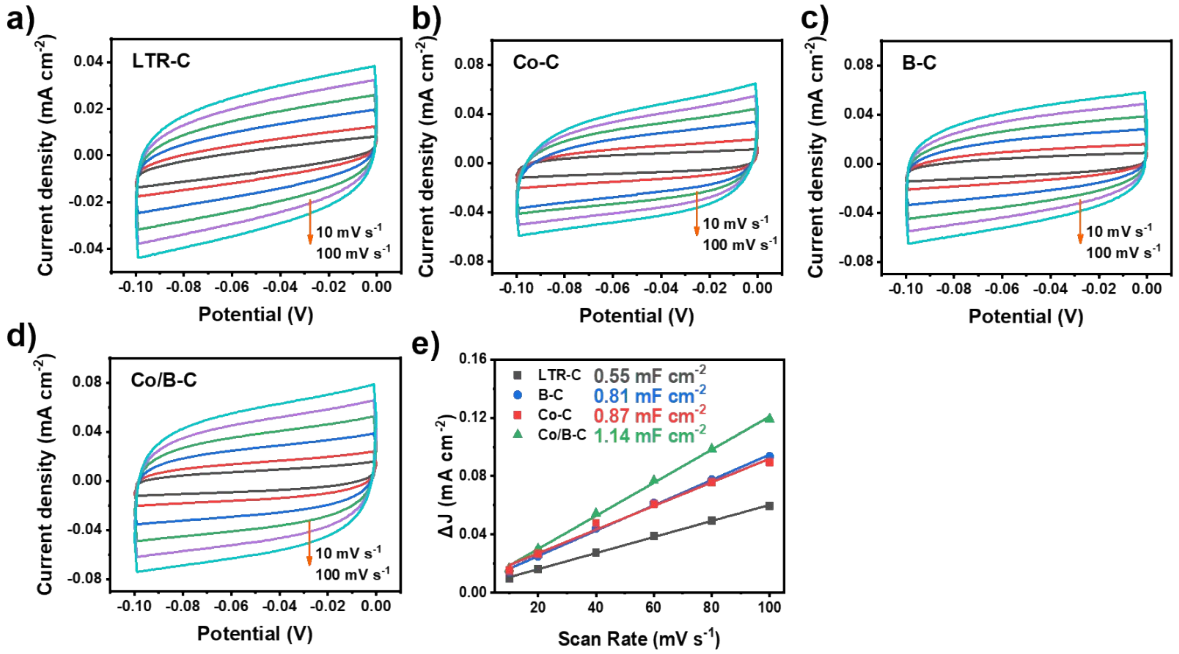

Fig. S19. CV curves of (a) LTR-C, (b) Co-C, (c) B-C, and (d) Co/B-C at various scan rates (10 to 100 mV s^{-1}) in range of - 0.10 to 0.00 V (e) C_{dl} of LTR-C, Co-C, B-C, and Co/B-C.

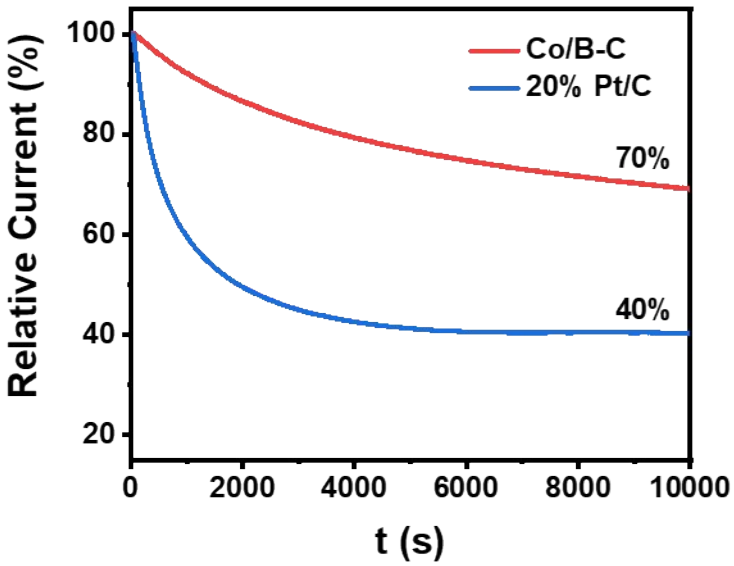

Fig. S20. Chronoamperometric responses of the hybrid Co/B-C and commercial 20% Pt/C catalysts in 1 M KOH for 10,000 s.

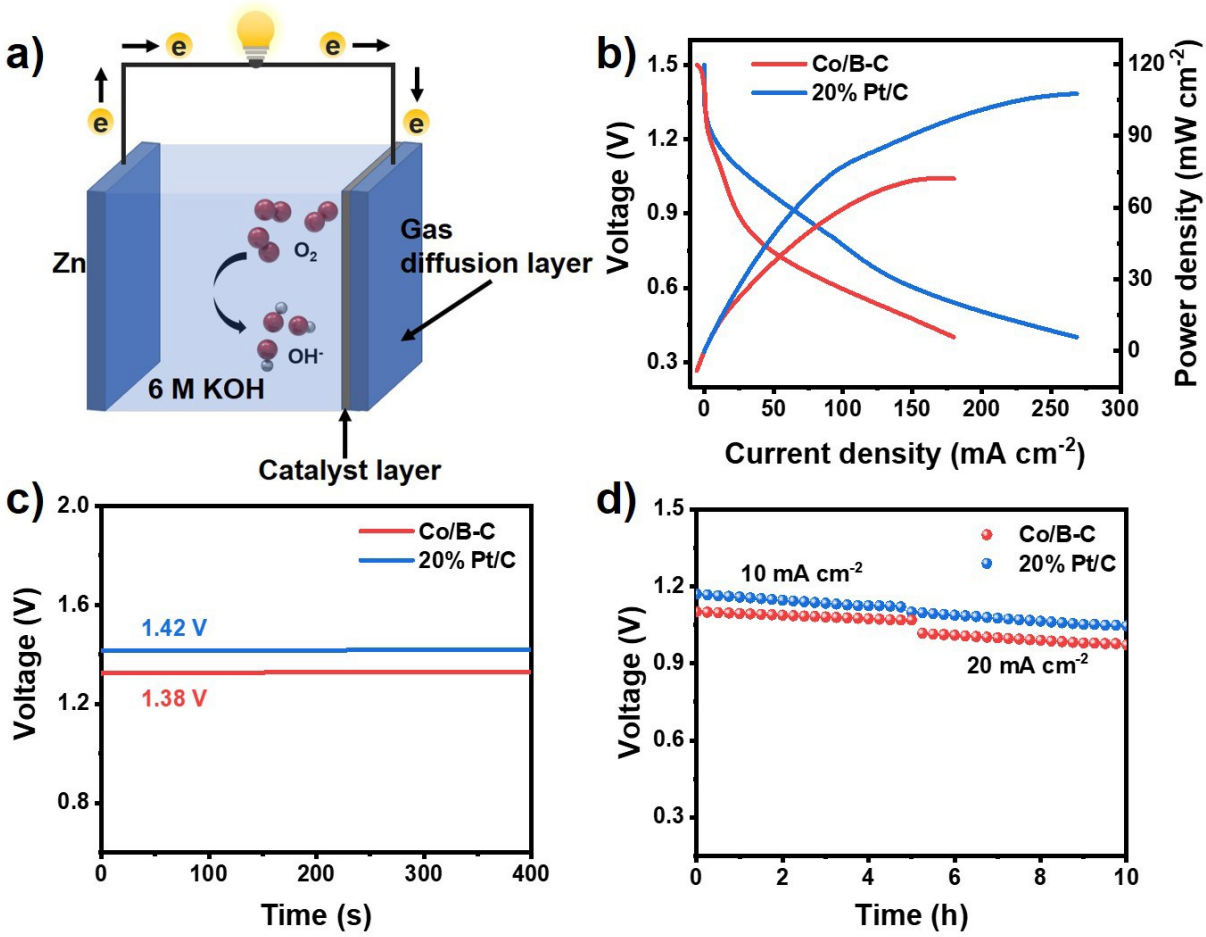

Fig. S21. (a) Schematic illustration of the Zn-air battery. (b) Discharge polarization curves and the corresponding power density curves of the Zn-air batteries made with Co/B-C and 20% Pt/C as cathode, respectively. (c) The open-circuit curves of Co/B-C and 20% Pt/C catalysts. (d) Discharge curves of the Zn-air batteries made with Co/B-C and 20% Pt/C as cathode at various current densities, respectively.

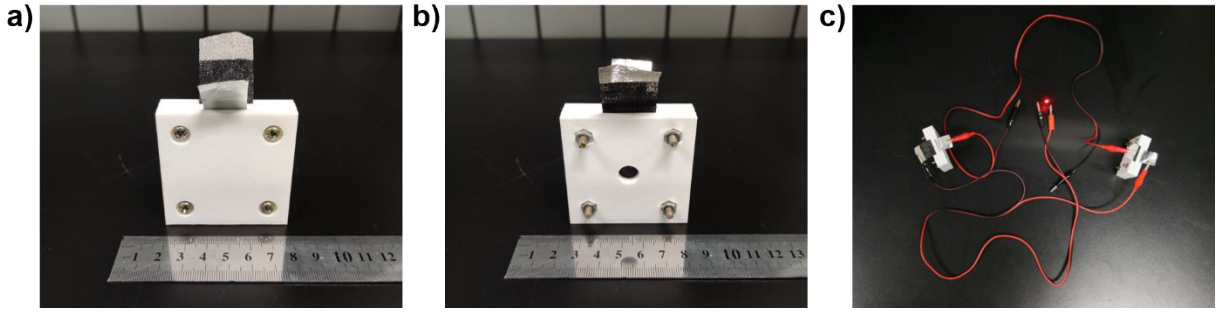

Fig. S22. (a,b) Photograph of the Zn-air battery built with a 3D printer. (c) Photograph of a red LED powered by two Zn-air batteries in series using Co/B-C catalyst as cathode.

4. Supplementary Tables

Table S1. The BET data of various catalysts.

Sample	Specific surface ($m^2 g^{-1}$)	Pore diameter (nm)	Pore volume ($mL g^{-1}$)
LTR-C	47.78	20.85	0.249
Co-C	35.14	18.60	0.163
B-C	22.81	53.64	0.305
Co/B-C	146.89	9.22	0.338

Table S2. The BET data of C/B-Co catalysts prepared with different laser power.

Laser power (W)	Specific surface ($m^2 g^{-1}$)	Pore diameter (nm)	Pore volume ($mL g^{-1}$)
9	30.67	23.98	0.184
12	34.24	23.93	0.205
15	46.37	25.16	0.292
18	146.89	9.22	0.338

Table S3. Comparison of the ORR performance of Co/B-C catalyst with other no-noble metal catalysts reported in the literature under alkaline conditions.

Sample	Onset potential (V)	Limiting current density (mA cm^{-2})	Tafel slope (mV dec^{-1})	Electrolyte	Ref.
Co/B-C	0.860	4.7	63	0.1 M KOH	This work
20% Pt/C	0.914	3.8	67	0.1 M KOH	This work
Co_3O_4/LIG	0.807	3.5	70	0.1 M KOH	[1]
NC-CNT-1000	0.840	6.8	85	0.1 M KOH	[2]
Co/NC	0.872	4.1	NA	0.1 M KOH	[3]
HGS-Mn_3O_4	0.827	6.3	73	0.1 M KOH	[4]
MnO_2/LIG	0.880	4.7	101	0.1 M KOH	[5]
LIG-O	0.770	3.6	90	0.1 M KOH	[6]
α-MnO_2-SF	0.880	4.8	NA	0.1 M KOH	[7]
GO-Zn/Co (2:1)-800	0.860	3.9	77	0.1 M NaOH	[8]

Notes and references

1. M. Ren, J. Zhang, J.M. Tour, Carbon, 2018, **139**, 880-887.
2. M. Qiao, S.S. Meysami, G.A. Ferrero, F. Xie, H. Meng, N. Grobert, M. Titirici, Adv. Funct. Mater., 2018, **28**, 1707284.
3. W. Xia, C. Qu, Z. Liang, B. Zhao, S. Dai, B. Qiu, Y. Jiao, Q. Zhang, X. Huang, W. Guo, D. Dang, R. Zou, D. Xia, Q. Xu, M. Liu, Nano Lett., 2017, **17**, 2788-2795.
4. X. Lv, W. Lv, W. Wei, X. Zheng, C. Zhang, L. Zhi, Q. Yang, Chem. Commun., 2015, **51**, 3911-3914.
5. M. Ren, J. Zhang, C. Zhang, M.G. Stanford, Y. Chyan, Y. Yao, J.M. Tour, ACS Appl. Energy Mater., 2020, **3**, 1702-1709.
6. J. Zhang, M. Ren, L. Wang, Y. Li, B.I. Yakobson, J.M. Tour, Adv. Mater., 2018, **30**, 1707319.
7. Y. Meng, W. Song, H. Huang, Z. Ren, S.-Y. Chen, S.L. Suib, J. Am. Chem. Soc., 2014, **136**, 11452-11464.
8. W. Yang, G. Chata, Y. Zhang, Y. Peng, J.E. Lu, N. Wang, R. Mercado, J. Li, S. Chen, Nano Energy, 2019, **57**, 811-819.